ANNUAL REVIEWS

Annual Review of Nuclear and Particle Science

Advances in Bolometer Technology for Fundamental Physics

S. Pirro[1] and P. Mauskopf[2]

[1]INFN, Laboratori Nazionali del Gran Sasso, L'Aquila I-67100, Italy; email: Stefano.Pirro@lngs.infn.it

[2]Department of Physics and School of Earth and Space Exploration, Arizona State University, Tempe, Arizona 85287; email: Philip.Mauskopf@asu.edu

Annu. Rev. Nucl. Part. Sci. 2017. 67:161–81

First published as a Review in Advance on July 31, 2017

The *Annual Review of Nuclear and Particle Science* is online at nucl.annualreviews.org

https://doi.org/10.1146/annurev-nucl-101916-123130

Keywords

cryogenic detectors, dark matter, double-β decay, cosmic microwave background, TES multiplexing

Abstract

In the last decade, cryogenic bolometers have provided increasingly improved resolution and sensitivity in particle and radiation detectors. Thermal particle detectors have proven their outstanding capabilities in different fields of fundamental physics, especially in rare event detection. Cryogenic incoherent detector arrays designed to detect millimeter-wave photons have helped enable precision measurements of anisotropies in the cosmic microwave background (CMB), providing a unique probe of early universe physics and helping to constrain parameters of particle physics such as the sum of the neutrino masses. We review the latest achievements of cryogenic particle detectors for direct detection searches for dark matter and double-β decay, as well as for CMB measurements, and we discuss expected improvements aiming to increase the sensitivities of these experiments. An important challenge is the large-scale implementation of arrays of detectors such as transition edge sensors, especially in CMB polarization experiments. We describe the challenges of scaling up to these larger arrays, including fabrication throughput and development of new multiplexing electronics.

Contents

1. INTRODUCTION

The history of thermal detectors begins in 1878, when Samuel P. Langley (1) invented the bolometer (from $\beta o \lambda \acute{\eta}$, "ray," and $\mu \acute{\epsilon} \tau \rho o \nu$, "measure") to measure the spectral distribution of energy from the Sun. After some improvements, the bolometer, working at room temperature, was able to measure a temperature change of one-hundred-millionth of a degree Fahrenheit—it was able to detect the presence of a cow in a pasture by the heat she radiated, even at a distance of a quarter of a mile (2).

The first detection of single α particles with a cryogenic bolometer was performed in 1949 (3) with a superconducting $3.5 \times 0.4 \times 0.006$ mm NbN layer at 15 K. It was, however, due to the development of doped germanium crystals (4) and their implementation as infrared bolometers (5) that the use of low-temperature detectors (LTDs) began to generate interest in the astronomical community. After the discovery of the cosmic microwave background (CMB) in 1965, germanium-based bolometers began to be integrated into millimeter-wave instruments designed to characterize the CMB anisotropies. Early (pre-2000) experiments used either coherent receivers, which could operate at temperatures of around 20 K (6–14), or small numbers of bolometers (15–21). Over time, the advantages in sensitivity and scalability of bolometer-based systems made them the primary technology in current and future CMB experiments, especially at measurement frequencies higher than 90 GHz.

Since 2000, superconducting transition edge sensors (TESs) have replaced germanium thermometers as the standard technology for CMB bolometer pixels because of their ability to be read out using superconducting quantum interference device (SQUID) multiplexing electronics and to be integrated into arrays with larger pixel counts. Superconducting kinetic inductance detectors (KIDs) are another direct detector technology that can be scaled to large-format arrays; they are also being used in several millimeter-wave ground-based experiments and could be suitable for use in next-generation CMB experiments. Significant milestones in the development of bolometric receivers include the characterization of the spectrum of the CMB by the FIRAS experiment (22); measurements of the degree-scale temperature anisotropies by the BOOMERANG and MAXIMA experiments (23, 24), which determined that the Universe is flat and provided strong support for the existence of dark energy; cosmic variance–limited characterization of the

temperature anisotropy; high signal-to-noise measurements of the E-mode polarization by the Planck, South Pole Telescope (SPT), and Atacama Cosmology Telescope (ACT) experiments (25–27); and detection of B-mode anisotropy by the BICEP2 and POLARBEAR experiments (28, 29).

With respect to nuclear and particle physics, however, it was in the late 1980s and early 1990s that LTDs began to be applied to rare event searches (30). LTDs soon demonstrated their superior capabilities with respect to standard particle detectors. A clear boost for these surveys, however, occurred around 2000 as a result of three separate events. The first two, both in 1998, were the discovery of neutrino oscillations (31) and the DAMA experiment's claim of a weakly interacting massive particle (WIMP) dark matter (DM) discovery (32). The third, in 2001, was the controversial claim of zero-neutrino double-β decay (DBD) (33), which was ruled out a decade later (34).

The advantage of LTDs over conventional detectors has long been established (35, 36). Specifically, LTDs have an improved detection threshold and better energy resolution, and a wide variety of materials can be used to produce them. The vast majority of the detectors used in nuclear and subnuclear physics have a common working principle: to measure the energy released along the path of an ionizing particle through a material. Such a signal is intrinsically limited by the fact that only a small fraction of the energy of the particle is involved in the ionization and excitation processes, as most of it goes into the production of heat and, as such, is lost. More importantly, however, the interaction of the particle with the detector produces a number of finite events or elementary quanta (e.g., electron–hole pairs in a semiconductor or photons in a scintillator), proportional to the energy deposited by the particle and inversely proportional to the mean energy necessary for the production of each of these quanta. In the case of germanium and silicon semiconductors, the average energy needed to produce an electron–hole pair is of the order of 2.9 and 3.6 eV, respectively, whereas the best energy resolution obtained so far for semiconductor X-rays detectors is of the order of 125 eV FWHM (37) (evaluated at 6 keV). In an LTD, however, the elementary quantum is represented by the phonon, whose energy can be orders of magnitude smaller (the maximum phonon energy is given by the Debye cut frequency, which is between 10 and 100 meV for most materials). Provided that the temperature is sufficiently low, multikilogram bolometers can be easily operated (38) with FWHM energy resolutions below 0.3% in the energy region of order (1 MeV).

Several comprehensive reviews of particle LTDs have been published. These include a very general description of different types of LTDs, using different sensor approaches (39), as well as an account of the latest developments on TESs for advanced X-ray detection (40).

2. LOW-TEMPERATURE DETECTORS FOR RARE EVENT PHYSICS

The ability to construct LTDs from a wide variety of materials is one of the important advantages of this technology. It can be fully exploited, for example, to search for very rare α decays using the so-called source-detector technique, as in the case of the α decay of ^{209}Bi with a half-life $T_{1/2} = 1.9 \times 10^{19}$ years (41), the α decay of ^{209}Bi to the first excited level (42), and the recently discovered α decay of ^{151}Eu (43).

Nonetheless, LTDs present practical challenges. First, they can be operated only at cryogenic temperatures (in this review, we focus only on detectors working between 10 and 300 mK) and must be enclosed within a series of four to six thermal radiation shields in ^{3}He–^{4}He dilution cryostats that—in the best-case scenario—take 1 day to reach the operational temperature. Moreover, depending on the mass, operating temperature, and type of phonon sensor, the duration of a thermal pulse can last from a few milliseconds to a few seconds, which can introduce problems

arising from pileup from natural radioactivity[1] and from cosmic rays. These problems can be overcome (in several cases) only by operating the detectors deep underground.

The second challenge relates to the fact that LTDs measure very tiny temperature differences over a stable base temperature. Variation in the base temperature will result in unwanted fluctuations in the response of the detector. Such temperature variations can come from different sources and frequently present a significant challenge for DM and DBD searches. The whole cryogenic facility may also be responsible for unwanted noise that originates from the mechanic–acoustic vibrations induced either by moving parts of the setup (pumps, compressors, cryocoolers) or by the flow and evaporation of the cryogenic fluid itself (44, 45). Such vibrations can work in two different ways: (*a*) They can generate energy deposition in the absorbers (46) that can drastically degrade the energy resolution of the detectors or (*b*) they can generate microphonic noise on the readout cables (47, 48).

Very often, these two processes are interconnected, even if their effects on the detectors are rather different. In the case of pure microphonic noise, in which the noise arises only from the vibration of the readout wires, thanks to adaptive/optimum filtering (49, 50) both energy resolution and energy threshold (51) can be efficiently improved, provided that the stochastic microphonic noise spectrum consists of semidiscrete peaks and the signal bandwidth consists of a continuum spectrum. In the case of thermal noise that is directly injected into the absorber, the situation is rather more problematic.

Unlike other kinds of surveys, both DM and DBD experiments consist of searches for single events on top of a large number of background events induced by natural radioactivity and other sources. At present (as discussed in more detail in Sections 2.1 and 2.2, below), the aim is to operate detectors in an almost-zero background mode, increasing as much as possible the exposure (mass of detectors multiplied by time of measurement). Doing so requires recognizing and disentangling background events through very sophisticated particle identification techniques. In the case of DM searches, this is presently the most limiting factor because the data analysis is performed mostly on threshold, where microphonic and thermal noise play a crucial role. In fact, in all of the recent results obtained by LTDs in DM searches, the best sensitivities were obtained only with a small subset of detectors or with a small part of the acquired data, or both (52–54). The problem of the vibrations and the excess noise generated by the cryogenic facility represents the *fil rouge* of these experiments. Generally there are two strategies to overcome these problems: attempt to decrease and damp the vibrations generated by the facility (55–57) and/or decrease the vibrations reaching the detectors by mechanical decouplings (e.g., through a pendulum-like structure and/or springs) between the cryostat and detector holders (58–62).

Moreover, all of these searches have a second common noise source: background events induced by natural environmental radioactivity. This means that all of the materials close to the detectors, as well as the detectors themselves, have to be fabricated from radiopure materials. In several cases, this results in serious limitations in the use of materials (e.g., readout cables, supporting materials, and the detectors themselves). Finally (as discussed in Sections 2.1.1, 2.1.2, and 2.2, below), the common challenge presently facing these detectors involves discriminating (background) events taking place at their surface. Addressing this challenge is the goal of next-generation experiments.

[1] By natural radioactivity we mean particles arising from trace contamination (e.g., ^{238}U and ^{232}Th) in the materials surrounding the detectors as well as within the detectors themselves.

2.1. Dark Matter Detectors

In the era of precision cosmology (63), we know that DM is five times more prevalent than baryonic matter in the Universe, and experimental evidence of DM has so far relied solely on indirect measurements of the effects of DM on gravitational interactions. Among a long list of hypothetical new particles, WIMPs with a mass in the (GeV–TeV)/c^2 region and weak-scale interactions naturally provide a relic density that matches that from astrophysical observations. The participation of such particles in weak-scale interactions would also enable direct detection in Earth-bound detectors via the process of elastic scattering off atomic nuclei (64).

Because the expected recoil energies are in the keV to sub-keV regime, depending on the mass of the DM particle and the target material, the challenge of such direct searches is to combine an ultralow background with a highly sensitive detection apparatus. Direct searches (65) are designed to register signals in the detector induced by the interacting particles in the form of scintillation, charge, and/or phonon signals. In the case of LTDs, the phonon signal is used to determine the total energy released in the absorber by the incident particle, whereas the second channel (ionization or scintillation) is used to determine the nature of the interacting particle. Neutral particles (e.g., WIMPs) show a lower ionization/scintillation signal compared with charged particles depositing the same amount of energy in the phonon channel. In a semiconductor detector, the ionization yield for nuclear recoils (i.e., WIMPs) is approximately 30% that of charged particles, whereas the scintillation yield of neutral particles in standard scintillators can be ~5–15% that of charged particles.

The use of LTDs for DM searches has recently changed due to the rapid progress of liquid noble-gas cryogenic experiments (66–69). These experiments have been able to make extraordinary improvements in particle identification, energy threshold, radioactivity levels, and most importantly the active mass of the detector (~1 ton). As a result, LTDs for DM searches have focused on the parameter space that is (and will be) inaccessible to conventional massive detectors, the region of light WIMPs with masses of <5–10 GeV/c^2. This implies enhancement of the energy threshold toward the keV and, ultimately, the sub-keV region.

Recent results obtained with LTDs are very impressive in terms of both energy threshold and background rejection. However, this progress has also identified new challenges not only in detector operation but also in the physics governing rare processes at low temperatures. In fact, whereas the signals in conventional detectors are induced by ionization processes, the signals in LTDs are induced by phonons. Unfortunately, there are other processes that can produce an almost pure phonon signal (70). Fractures and/or relaxations of the crystal absorber lattice can induce phonon signals that can mimic the DM interaction because the ionization/scintillation signals are absent or extremely weak (52, 71). In some cases, these relaxations occur in a sudden burst, with some decay constants that can last a few days (52). Current and expected research and development on these detectors will involve further reducing the energy thresholds (down to tens of eV) and attempting to fully understand and mitigate the effect of spurious phonon signals that can limit background discrimination.

2.1.1. Ionization–heat low-temperature detectors. Ionization–heat LTDs make use of undoped silicon and germanium crystals, both as crystal absorbers and as ionization detectors. At milli-Kelvin temperatures, effectively, all free electric carriers are completely frozen out so that there is no need to create a depletion layer as in conventional (i.e., doped) silicon and germanium diodes. The charge generated by ionizing particles can be easily collected by means of ohmic contacts.

The use of ionization–heat detectors for DM searches provides several advantages. Both germanium and silicon crystals have a large industrial market, so their development as pure and single (perfect) crystals is well established. Moreover, unlike other types of crystals used in this field, they can have extraordinary radiopurity (72). Finally, thanks to the Neganov–Trofimov–Luke effect (73, 74), the phonon signal can be amplified by a suitable electric field with the possibility to lower the energy threshold to unprecedented values (see Section 2.3).

As mentioned in the previous section, the key development for these detectors was and is the discrimination of surface events. Particle interactions taking place on the surface of the detector (a few tens of micrometers, equivalent to β/γ events up to 10–20 keV) will unavoidably suffer from incomplete charge collection in a similar (but different) way as occurs in conventional germanium diodes. Because the total phonon pulse height does not depend on position, the incomplete charge collection for surface events mimics the interaction of a neutral particle, such as the WIMP signal. In the remainder of this section, we review the results obtained by two collaborations exploiting this technique: Edelweiss (75) and SuperCDMS (76).

The Edelweiss Collaboration developed cylindrical germanium crystals (~800 g each) with a very powerful charge collecting scheme by using fully interleaved digitized (FID) electrodes—that is, a series of interleaved concentric aluminum electrodes (alternately biased) that also extends laterally (**Figure 1*a***). The fiducial electrodes collect the charge of events releasing energy inside the detector while charge depositions taking place a few millimeters from the surfaces are tagged by signals on a veto electrode. The full detector thus comprises two temperature sensors [neutron transmutation doped thermistors (NTD) (77)] and four types of collecting electrodes. The corresponding charge collecting field produces a sort of fiducial (inner) volume (~75% of the total volume) in which the charge produced close to the boundary cannot diffuse: Charges from surface events will drift to the same-side (oppositely biased) electrodes, whereas the charges produced in the bulk perceive the stronger potentials from the fiducial electrodes. From the

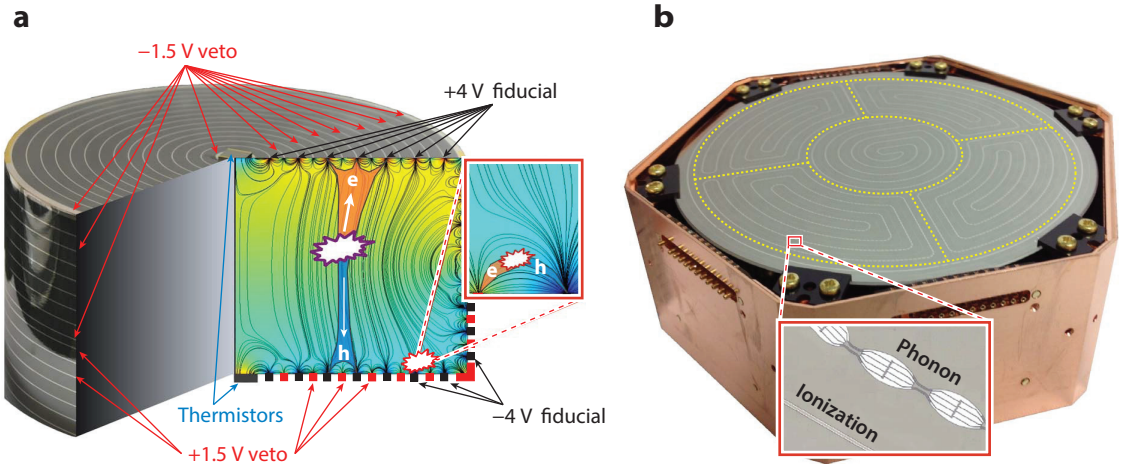

Figure 1

(*a*) The bare 800-g Edelweiss-III full interleaved detector (FID) (70 mm in diameter, 40 mm high) with a pictorial view of the inner electric field lines as derived from numerical calculations. (*b*) The 1.4-kg SuperCDMS germanium interleaved *Z*-sensitive ionization phonon (i-ZIP) detector (100 mm in diameter, 33 mm high) that will operate at SNOLAB (80). The yellow lines are intended to guide the eye and point out the six lithographically deposited transition edge sensor structures. (*Inset*) Image of the ionization and phonon rails. Panel *a* modified with permission from the Edelweiss Collaboration. Panel *b* modified with permission from the SuperCDMS Collaboration.

independent readout of the four electrodes, a very powerful surface-event discrimination can be performed.

The temperature sensors are NTDs, one on the top and the other on the bottom of the flat faces, operated at temperatures close to 20 mK. The main sensitivity limitation of these detectors is related to the presence of heat-only events (52). These events, as discussed above, could originate from mechanical or fracture processes (both internal and external to the fiducial volume) and mimic potential WIMP-induced recoils for which the deposited energy is large enough to be triggered by heat channels but the quenching is too small to generate a detectable fiducial ionization signal. The use of two independent thermistors assists in the rejection of spurious noise that could be generated, for example, by microfractures induced by the glue used to couple the thermistors to the germanium absorber. In this case, the heat signal will prevail on the sensor close to the glue, whereas true WIMP signals will have to show the same pulse height on both thermistors.

The SuperCDMS Collaboration uses both germanium and silicon detectors. The use of different target nuclei in the same setup permits a better understanding of the induced backgrounds at very low energies, especially those induced by possible environmental neutrons that will show different energy spectra in the two types of detectors. In this case, the temperature sensors are a series of TESs patterned on the top and bottom parts of the crystal (78). The working temperature of the detectors is between 55 and 62 mK. The main advantage with respect to semiconductor thermistor-based devices is that the TESs are sensitive to ballistic phonons (i.e., the phonons propagating almost straight from the impact position of the particle), so that some important information about the position of the event is contained in the pulse shape and arrival time measured by the independent TES channels. The charge collecting electrodes (operating at approximately +2 V on the top and approximately −2 V on the bottom) are interleaved with the TES strings and kept at 0 V in order to disentangle surface events, similar to the process discussed above. There are no electrodes on the lateral side of the detector, and in order to disentangle surface events, the top and bottom of the electrodes consist of an inner (fiducial) electrode and an outer (guard) electrode (**Figure 1*b***). Each detector has six TES phonon channels on each side, arranged as an inner core, surrounded by four wedge-shaped channels and one outer ring. An outer ionization channel shares the same area and is interleaved with the outermost phonon ring, and an inner ionization channel is interleaved with the remaining phonon channels. An individual detector thus consists of 12 TES channels and 4 ionization readouts. The Edelweiss and SuperCDMS Collaborations have similar root-mean-square (rms) baseline energy resolutions (75, 76) of 200–400 eV for both heat and ionization channels.

Both experiments make use of statistical algorithms to minimize the energy threshold and to reject the background induced by environmental radioactivity and false heat-only pulses. Both experiments end up with a boosted decision tree algorithm whose training makes use of several input parameters, such as simulated background events, neutron calibration events, and a simulated WIMP nuclear recoil spectrum. This algorithm, performed individually for each detector, reveals very small efficiencies that, on threshold (between 1 and 1.6 keV for both experiments), can reach values below 5% (75, 76). These cumulative cuts—even if characterized by rather small efficiencies on the background data—are able to reject a large fraction of non-DM events, resulting, finally, in an overall increase in sensitivity for DM searches.

Two major improvements are expected in the very near future. First, the noise in the charge readout channel could be improved by a factor of approximately three by use of high–electron mobility transistor (HEMT) amplifiers instead of the standard junction gate field effect transistor (JFET) amplifiers that are presently in use. This would enable an ionization rms of the order of 100 eV (79, 81). Furthermore, JFETs require an operating temperature above 80 K, whereas HEMTs natively operate at ∼4 K; therefore, the complexity of the readout scheme, as well as the

cable links from detectors to the first ionization amplification stage, can be significantly reduced. Second, the use of the Naganov–Trofimov–Luke amplification (see Section 2.3) could reduce the heat energy threshold by more than one order of magnitude.

2.1.2. Scintillation–heat bolometers. The use of the scintillation signal to reject natural radioactivity provides several advantages with respect to germanium and silicon heat–ionization devices. For example, different nuclei constituting a crystal will produce a slightly different scintillation signal depending on which nucleus is hit by the impinging particle (82). The expected WIMP recoil spectrum (assuming coherent scattering) will therefore show different features depending on the mass of the WIMP particle. In the case of $CaWO_4$ crystals, used by the CRESST experiment (83), the WIMP energy spectrum will be completely dominated by tungsten scatters for WIMP masses above 20 GeV/c^2; at the same time, the light targets (calcium and, especially, oxygen) make these detectors particularly sensitive to WIMP masses of the order of a few GeV/c^2. Furthermore, knowledge of the recoil composition of different constituents could also enable a test of the assumed dependence—$\propto$(atomic mass)^2—of the spin-independent WIMP–nucleon cross section. Moreover, the environmental background induced by neutrons (visible mainly as oxygen scatters for reasons of simple kinematics) could be statistically discriminated. In addition, the possibility to choose and, in the case of a positive signal, to switch between a large number of target nuclei could permit a search for different types of possible couplings, such as spin-dependent interactions. From this point of view, the extreme versatility in the choice of the target material makes this technique very powerful.

The CRESST experiment is presently running its third phase: an array of 10 modules, each consisting of a $CaWO_4$ crystal absorber and its light detector (**Figure 2**). In order to eliminate events induced by surface radioactivity, all of the materials inside the copper detector housing are fabricated from scintillating materials. This is crucial, especially for the rejection of nuclear recoils produced by surface α emitters, which can mimic DM particle recoils. The few-MeV α particles

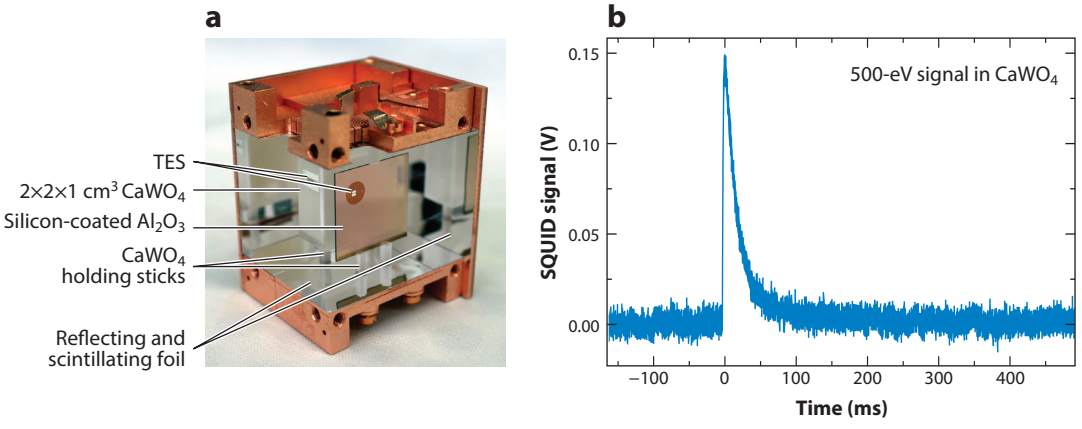

Figure 2

(*a*) The 24-g CRESST-III detector module (84) with part of the reflective and scintillating housing removed. The light detector consists of a very sensitive Al_2O_3 crystal bolometer that shows baseline resolution of the order of 4–10 eV (approximately two to four scintillation photons). Both the phonon and light detectors are held by scintillating $CaWO_4$ sticks. (*b*) A typical 500-eV pulse in the absorber, recently obtained by the running experiment at Gran Sasso, that shows the extremely high energy sensitivity that can be reached by these detectors; 1 out of the 10 modules of CRESST shows an impressive energy threshold of 25 eV (83a). Abbreviations: SQUID, superconducting quantum interference device; TES, transition edge sensor. Modified with permission from the CRESST Collaboration.

emitted in the decay will produce enough light in the scintillating materials to veto this harmful background very efficiently. CRESST absorber crystals are kept in position by so-called iSticks, which, as the main absorber, are made from $CaWO_4$. Particle interactions or stress relaxation events taking place in these holding sticks also transfer a small fraction of the total energy deposit to the main absorber via the tiny contact area. Because such events could mimic potential DM interactions, the sticks are equipped with TESs, thereby providing a reliable and active veto against such sources of background.

The COSINUS experiment (85) was recently proposed; it will use NaI heat–scintillation bolometers to directly test the DAMA/LIBRA claim (86). The first tests, obtained with CsI crystals, are very promising (87), and the final experiment conducted with NaI crystals will not only cross-check the claim but also aid our understanding of the nature of the interacting particle, thanks to the different scintillation quenching.

The heat–scintillation technique, although very versatile with respect to heat–ionization devices, has some different limitations. The first involves the intrinsic radiopurity of scintillating crystals. Even in the presence of very accurate particle identification, internal radioactive contamination remains an important bottleneck, the solution to which requires not only time but also developments in both material selection and crystal growing techniques that—in contrast to semiconductors—have no reasonable market application. The second drawback is that, unlike semiconductors, this technique cannot make use of the Neganov–Trofimov–Luke heat signal amplification (discussed in Section 2.3). Therefore, the only way to significantly improve the energy threshold is to reduce the mass of the absorbers. The mass ratio of the SuperCDMS germanium single detector with respect to the CRESST single module is 1,400 g/24 g ≈ 60.

2.2. Double-β Decay Low-Temperature Detectors

Neutrinoless DBD (88) represents one of the best probes to test lepton number conservation and allows for the investigation of the nature of the neutrino mass eigenstates. Searches for this decay have been performed for decades, investigating a wide variety of nuclei with many different experimental techniques (89). The experimental signature is in principle very clear: One should expect a sharp peak at the $Q_{\beta\beta}$ value of the reaction (2–3 MeV for most of the interesting emitters) to be disentangled from a continuous background induced by natural radioactivity. Despite such a characteristic signal, the rarity of the processes under consideration makes their identification very difficult. Such remotely probable signals have to be disentangled from background arising from natural radioactive decay chains, cosmogenically induced activity, and human-made radioactivity, which deposit energy in the same region as the DBD but at a faster rate. Consequently, the main task in DBD searches is to decrease and (possibly) identify the induced background. Bolometers are ideal detectors for this purpose because of their excellent energy resolution, choice of materials (DBD emitters), and possibility of recognizing the nature of the interacting particle. In recent years, increased sensitivity was obtained through large-mass TeO_2 bolometers (90, 91).

The Cryogenic Underground Observatory for Rare Events (CUORE) detector (**Figure 3*a***) represents the ultimate challenge for this research: 988 TeO_2 crystal bolometers for a total active mass of $\sim$741 kg, operating at a temperature close to 10 mK. Similarly to DM LTDs, the major source of background for this survey is due to surface events (92): High-energy (4–6 MeV) α particles arising from surface contamination (from dead layers facing the detectors as well as the detectors themselves) can lose part of their energy and strike the crystal with the same energy as the DBD peak. The amount of contamination is so low ($\leq$ few 10^{-8} counts h^{-1} keV^{-1} cm^{-2}) that they cannot be measured—or even screened—with any standard device or technique.

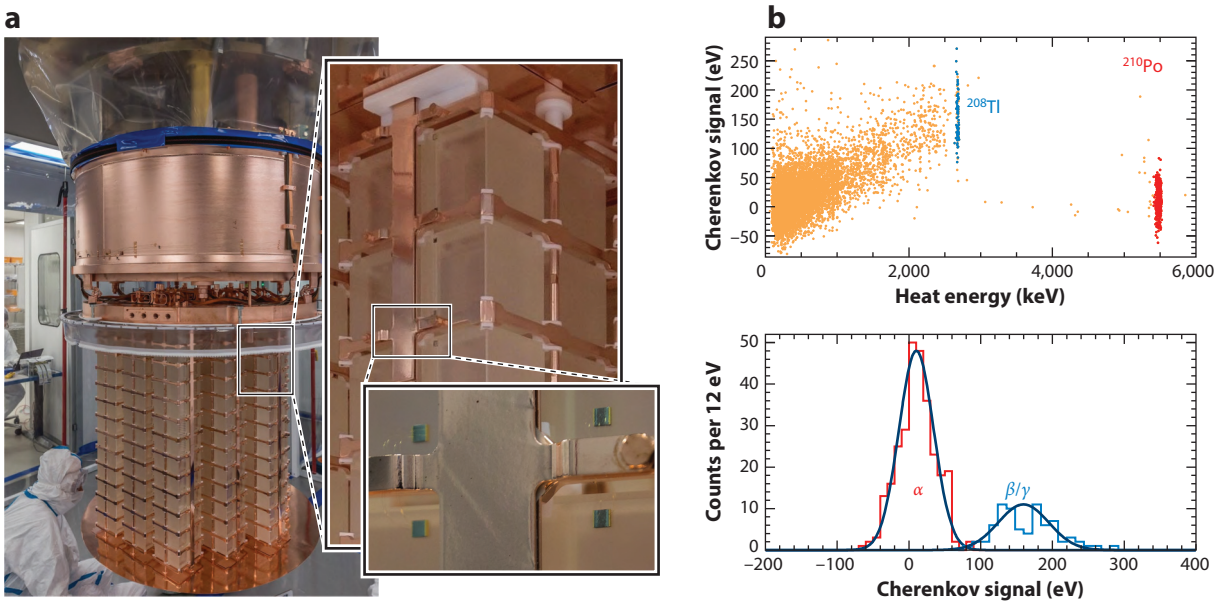

Figure 3

(*a*) The 988 TeO_2 crystals framed in 19 towers inside the CUORE cryostat. The entire setup is inside an airtight clean room flushed with low-radon-content air to prevent surface radioactive contamination induced by radon implantation. (*Insets*) Details of a single tower (*top*) and of the neutron transmutation doped thermistors coupled to the crystals (*bottom*). The detector was cooled down in December 2016, and the physical background run started in April 2017; the first preliminary results show that an average energy resolution of 7.9 keV FWHM at 2,615 keV has already been achieved (91a). (*b*) The α versus β/γ discrimination obtained with a 435-g, 95%-enriched $^{130}TeO_2$ crystal, thanks to the readout of the weak Cherenkov light emitted by electrons. The thermistor-based germanium light detector takes advantage of the Neganov–Luke amplification (113). Panel *a* modified with permission from the CUORE Collaboration.

To overcome this troublesome background, in 2005 researchers suggested (93) reading out the scintillation light through a second LTD, in the same way as for DM searches. Originally, the idea was to use scintillating DBD bolometers consisting of DBD emitters with high $Q_{\beta\beta}$ values (94–96) to simultaneously overcome both surface radioactivity and the most prominent natural high-energy radioactivity, induced by the line of ^{208}Tl, at 2,615 keV. Moreover, some scintillating crystals (e.g., ZnSe and molybdates) have a very peculiar feature: The thermal pulse induced by an α particle shows a slightly faster decay time than that induced by β/γ interactions. This feature can be explained (97) by the relatively long scintillation decay time (of the order of hundreds of microseconds) observed at cryogenic temperatures in some crystals (98). This long decay, combined with a high percentage of nonradiative de-excitations of the scintillation channel, will produce delayed phonons (i.e., heat) in the crystal. This extremely tiny, but measurable, time-dependent phonon release has different absolute values for isoenergetic α and β/γ particles due to their different scintillation yields. This means that, in principle, particle discrimination could be obtained in scintillating crystals without light detection. However, doing so requires a very good signal-to-noise ratio because this effect is rather small (99).

Several DBD experiments using scintillating and isotopically enriched crystals are being operated or constructed. CUPID-0 (100), formerly LUCIFER (101), is currently running using an array of 24 enriched $Zn^{82}Se$ crystals; AMORE (102) will use $^{dep}Ca^{100}MoO_4$ (or another molybdate such as $Zn^{100}MoO_4$ or $Li_2{}^{100}MoO_4$); and LUMINEU (103) will use an array of $Li_2{}^{100}MoO_4$ crystals.

2.3. Neganov–Trofimov–Luke Amplification

The so-called Neganov–Trofimov–Luke amplification, commonly called Neganov–Luke (NL) amplification, is based on the application of an electric field in a semiconductor cryogenic detector. The work performed by the field on the drifting electron–hole pairs (generated by the energy release of the impinging particle) is converted into additional heat, which can considerably amplify the thermal signal read by the phonon sensor. In the ideal case, the gain in terms of phonons can simply be written as

$$G = 1 + \frac{e\,\Delta V}{\epsilon}, \qquad 1.$$

where e is the electron charge, ΔV is the applied drift voltage across the electrodes, and ϵ is the mean energy needed to create an electron–hole pair (in germanium, this value is $\sim$3 eV). This mechanism is particularly interesting because the heat amplification can be used to substantially decrease the energy threshold. This mechanism can be explained as a sort of phonon avalanche induced by the electron–hole pairs accelerated by the field. The advantage is that, in principle, this avalanche is independent of any other source of noise. This effect is rather well known and is normally taken into account to correct the energy scale in heat–ionization detectors: Due to the different ionization yield, neutral particles will have a slightly different amplification so that the energy scale for nuclear recoils (WIMPs) has to be renormalized with respect to the β/γ scale.

This technique was recently applied, with excellent results, by the SuperCDMS Collaboration (53) in the CDMSlite experiment. Through the use of a large bias field ($\sim$70 V) on a germanium interleaved *Z*-sensitive ionization phonon (i-ZIP) detector, the effective threshold was lowered to 56 eV. The SuperCDMS Collaboration (80) plans to use eight germanium and four silicon detectors with NL amplification in the near future, with a projected phonon rms energy resolution of the order of $\sim$10 eV. The Edelweiss Collaboration (104) recently succeeded in operating an NL-amplified germanium detector with a field of 180 V and a heat gain of the order of $\sim$60. Note, however, that there is a clear drawback in this large heat amplification: The information about the heat–ionization ratio (fundamental for event discrimination) is washed out because at high gains the heat signal will simply be proportional to the ionization.

NL amplification, however, can be very effectively used to enhance the capabilities of bolometric light detectors. The use of NL amplification in this field began in 2005 with the goal of increasing the energy threshold of bolometric light detectors for heat–scintillation DM searches (105). However, the first tests were seriously limited by an increase in baseline noise due to the presence of the electric field, generating unwanted dark currents within the device. Later, in 2012, the first encouraging result was obtained with a silicon absorber and an iridium/gold bilayer TES, in which, thanks to NL amplification, an increase in the signal-to-noise ratio of approximately nine was obtained (106). A subsequent boost in research and development was driven by the possibility to read out the tiny amount of Cherenkov light from TeO_2 crystals in order to actively discriminate α particles in nonscintillating DBD crystals (107, 108). In the last 2 years, several NL-amplified devices were developed to read out the Cherenkov light from TeO_2 crystals: with silicon absorbers and TESs (109), with germanium absorbers and NTD (110), and with silicon absorbers and NTD (111). The most recent, very promising result, in view of CUPID (CUORE upgrade with particle identification) (112), was recently obtained (113) with NTD-based germanium NL-amplified devices coupled with 435 g of enriched $^{130}TeO_2$ crystals (**Figure 3*b***).

3. LOW-TEMPERATURE DETECTORS FOR NEUTRINO MASS EXPERIMENTS

In contrast to DBD searches, direct measurement of the (anti)neutrino mass through high-energy-resolution single-β decay spectroscopy does not rely on the nature of the neutrino

particle. The precise high-statistics measurement of the shape of the endpoint spectrum can measure the neutrino mass irrespective of its nature (Dirac or Majorana particle). In recent years, several pioneering experiments using ^{187}Re-based LTD microcalorimeters were developed (114) as an attractive alternative to tritium experiments (115).

Present-day experiments are focusing on ^{163}Ho electron capture driven mainly by the fact that ^{163}Ho has a relatively short decay time such that it can be implanted (as a sort of negligible doping) in standard high-energy-resolution X-ray microcalorimeters. The necessary compromise in this survey is the balance between having a very good energy resolution detector and a very fast rise time in order to get rid of pileup events that will spoil the shape of the β spectrum close to the endpoint.

The HOLMES experiment (116) will make use of molybdenum/copper TESs at a temperature of 100 mK. Due to the large number of TES channels expected for this experiment, the development of multiplexed readout is mandatory. Preliminary results with microwave radio-frequency (RF) multiplexed SQUIDs show energy resolution of the order of 5 eV with rise times of the order of 10 μs (117).

The ECHo experiment (118) will use metallic magnetic calorimeters (MMCs) at temperatures of the order of 50 mK. MMCs are the fastest LTDs developed to date, with rise times one order of magnitude shorter than those obtainable with TESs. In this case as well, the array will need a microwave RF multiplexed SQUID readout; recent microwave multiplexing devices (119) were able to measure rise times of the order of 90 ns, even though the energy resolution, which reached approximately 50 eV, needs further improvement.

4. LOW-TEMPERATURE DETECTORS FOR COSMIC MICROWAVE BACKGROUND PHYSICS

Observables in the CMB consist of anisotropies in both temperature and polarization, as well as distortions in the spectrum compared with an ideal blackbody. The amplitude of these effects ranges from $<10^{-9}$ to 10^{-4} of the CMB or, when expressed as a temperature variation, from nano-Kelvin to hundreds of micro-Kelvin. CMB measurements are compared with models that predict the properties of the different observables as a function of values for a set of parameters. These parameters include fundamental physics properties such as the DM and dark energy densities ($\Omega_{\rm dm}$ and Ω_Λ, respectively), the sum of the neutrino masses, and the effective number of light relativistic species ($N_{\rm eff}$). To date, no significant global spectral distortions have been detected (although local distortions from the Sunyaev–Zel'dovich effect toward galaxy clusters have been detected in a large number of objects).

Current anisotropy measurements can be fit to a minimal set of six parameters, namely the baryon density ($\Omega_b h^2$), the cold dark matter (CDM) density ($\Omega_c h^2$), the sound scale at recombination ($\theta_{\rm MC}$), the optical depth to recombination (τ), the index of scalar perturbations ($n_{\rm s}$), and the perturbation amplitude at a scale of 0.05 Mpc^{-1} ($A_{\rm s}$) (120). From these parameters it is possible to derive the value of other quantities, such as the Hubble constant (h) and the densities of matter (Ω_m) and dark energy (Ω_Λ). However, this model contains several assumptions, including that the sum of neutrino masses is equal to 0.06 eV, that there are no tensor fluctuations, and that the dark energy is in the form of a cosmological constant.

The lensing signal in the CMB can be extracted from the three-point correlation function of the temperature and E-mode anisotropy and from the B-mode anisotropy, and can provide a constraint on the neutrino masses through an effect on the evolution of large-scale structure. Primordial gravitational waves in the early Universe could also produce a B-mode polarization signal and a non-Gaussian distribution in the temperature or polarization anisotropies. Characterization

of the evolution of the number of galaxy clusters as a function of redshift and mass is one way of constraining the equation of state of dark energy. More precise measurements of the anisotropies will allow all of these effects to be explored in depth over the next decade. Improvements in these measurements will require better instrument sensitivity, mapping speed, and control of systematic effects.

4.1. Current Cosmic Microwave Background Experiments

Several ongoing CMB experiments are designed to characterize the polarization anisotropy from both ground-based and balloon-borne platforms. These include the BICEP/Keck experiments (121); SPT polarization experiment (122); POLARBEAR experiment (123); Cosmology Large Scale Surveyor (CLASS) (124); SPIDER, EBEX, and PIPER balloon-borne experiments (125–127); and ACT polarization (ACT-Pol) experiment (128, 129). All of these experiments have focal planes with on the order of 1,000–10,000 TES bolometers. The individual detector sensitivities are limited by the background loading from the instrument and the atmosphere, as the detector noise is typically comparable to the photon noise sensitivity limit. **Table 1** lists the basic parameters for some of the current CMB experiments.

Individual single-mode detectors in ground-based CMB experiments have achieved close to quantum limited sensitivity dominated by photon noise from background loading corresponding to approximately 300 $\mu K\sqrt{s}$. Balloon-borne instruments have achieved a sensitivity per detector that is approximately twice as high (e.g., SPIDER) (**Table 1**), which could improve by another factor of approximately 1.5, corresponding to a mapping speed advantage of a factor of 4–9. The ultimate single-mode sensitivity limit is from the photon noise in the CMB alone, which is approximately 50 $\mu K\sqrt{s}$ for a 30% band centered at a frequency near the CMB peak. This sensitivity is achievable with existing LTD technology operating from a base temperature of on order 100 mK. Therefore, the main focus for improvement in instrument sensitivity and speed is

Table 1 Parameters of transition edge sensor detectors from recent cosmic microwave background experiments[a]

Instrument (reference)	ν_{cen} (GHz)	$\Delta\nu$ (GHz)	P_{opt} (pW)	T_{base} (mK)	NEP_{det} ($aW/\sqrt{Hz}$)	Efficiency ($aW/\sqrt{Hz}$)	Sensitivity ($\mu K\sqrt{s}$)	N_{det}
CLASS40 (130)	38	10	1.7	70	8	0.58	211	72
CLASS90 (130)	90	30	4.0	70	12	0.48	180	1,036
ACT-MBAC (131)	148	28	4.0	300	54	0.25	890	1,024
BICEP2 (132)	150	43	4.7	270	38	0.38	320	512
SPIDER90 (125)	90	25	0.8	270	17	0.38	135	512
SPIDER150 (125)	150	38	0.8	270	17	0.38	130	512
ACT-Pol150 (133)	146	51	5.1	80	15	0.25	320	2,558
POLARBEAR (134)	148	34	6	250	83	0.35	745	1,274
SPT100 (135)	98	31	7.3	280	33	0.1	1,540	960
SPT150 (135)	155	35	7.5	280	33	0.15	1,340	960
SPT220 (135)	220	49	17	280	40	0.14	3,100	960
SPTPol-90 (136)	91	30	10	280	35	0.33	620	360
SPTPol-150 (136)	146	43	9.2	280	49	0.34	530	1,176

[a] ν_{cen} is the approximate band center, $\Delta\nu$ is the bandwidth, P_{opt} is the typical optical power absorbed by the detector, T_{base} is the focal plane base temperature, NEP_{det} is the detector noise-equivalent power or sensitivity to a change in absorbed power in a 1-s integration, and N_{det} is the number of detectors in the instrument.

increasing the system throughput (product of the telescope aperture, A, and the instantaneous field of view, Ω) and, therefore, the number of modes: $N_{\text{modes}} = A\Omega/\lambda^2$. This increase in throughput requires an increase in either detector size (for multimode detectors) or number of detectors (for single-mode detectors). Single-mode detectors can also provide the highest angular resolution when coupled to a fixed telescope aperture. Future ground-based CMB experiments are planned to have a 10–100-fold increase in throughput and number of detectors. Fielding 10^5–10^6 LTDs requires new developments in detector fabrication and readout.

4.2. Fabrication of Large Low-Temperature Detector Arrays

State-of-the-art CMB TES arrays come in three variations of optical coupling: (*a*) planar antenna phased arrays (e.g., the BICEP/Keck arrays), (*b*) horn-coupled arrays (e.g., AdvancedACT-Pol and CLASS arrays), and (*c*) lens/antenna arrays (e.g., the Simons and SPT-3G arrays), each of which contains approximately 1–10,000 detectors. The BICEP/Keck detectors are planar slot antenna arrays connected by superconducting transmission lines, then coupled to TES detectors to form pixels with directed beams in two polarizations with band-pass filters all on-chip. The AdvancedACT-Pol and CLASS detectors consist of planar superconducting wave-guide probes coupled to superconducting planar transmission lines, which enable the signals to be divided into the two polarizations, as well as multiple frequency bands on-wafer before being coupled to the TES detectors. The wave-guide probes are fed by direct machined profiled horns or silicon micromachined horn arrays (**Figure 4**). The detectors for the Simons and SPT-3G arrays are planar antennas coupled to lenslet arrays and incorporate on-wafer polarization separation and filtering. All of these detector types and plans for scaling them up to arrays of 10^5–10^6 pixels are described in detail in the CMB-S4 instrument book (see **https://cmb-s4.org/**).

Fabrication of these detectors requires new approaches to reduce the cost and time per detector. Areas under investigation include increasing wafer sizes from typically 4 inches to 6 inches and transferring fabrication technology to multiple fabrication centers in both research and commercial institutions.

Another approach to increased detector counts is to use a different LTD technology—KIDs—to decrease the complexity of the detector design, fabrication, and multiplexing processes. KIDs are superconducting resonators that change their resonant frequency in response to absorbed incident radiation. A large array of direct absorbing or lumped element KIDs (LEKIDs) can be fabricated with a relatively small number of processing steps compared with a TES array, and KID focal planes have been used in ground-based astronomical instruments at frequencies ranging from 150 GHz to 1 THz (139–141). In addition, polarization-sensitive KIDs are planned for use in ground-based instruments at frequencies ranging from 150 to 300 GHz (G. Wilson & A. Monfardini, personal communication) and on the BLAST and STARFIRE balloon-borne far-infrared instruments (142, 143). Although promising results have been obtained for dual-polarization KIDs in the laboratory (144), KIDs have not yet been deployed in a CMB polarization experiment.

4.3. Readout of Large Low-Temperature Detector Arrays

The development of cryogenic multiplexing electronics for the readout of arrays of LTDs has enabled the current generation of CMB experiments to have on the order of 10,000 detectors. The two main readout electronics systems for TES bolometers in use today are time-division multiplexing (TDM) (146, 147) and frequency-division multiplexing (FDM) (148), both of which use SQUID current amplifiers. **Figure 5** depicts the basic schematics of TDM and FDM readout

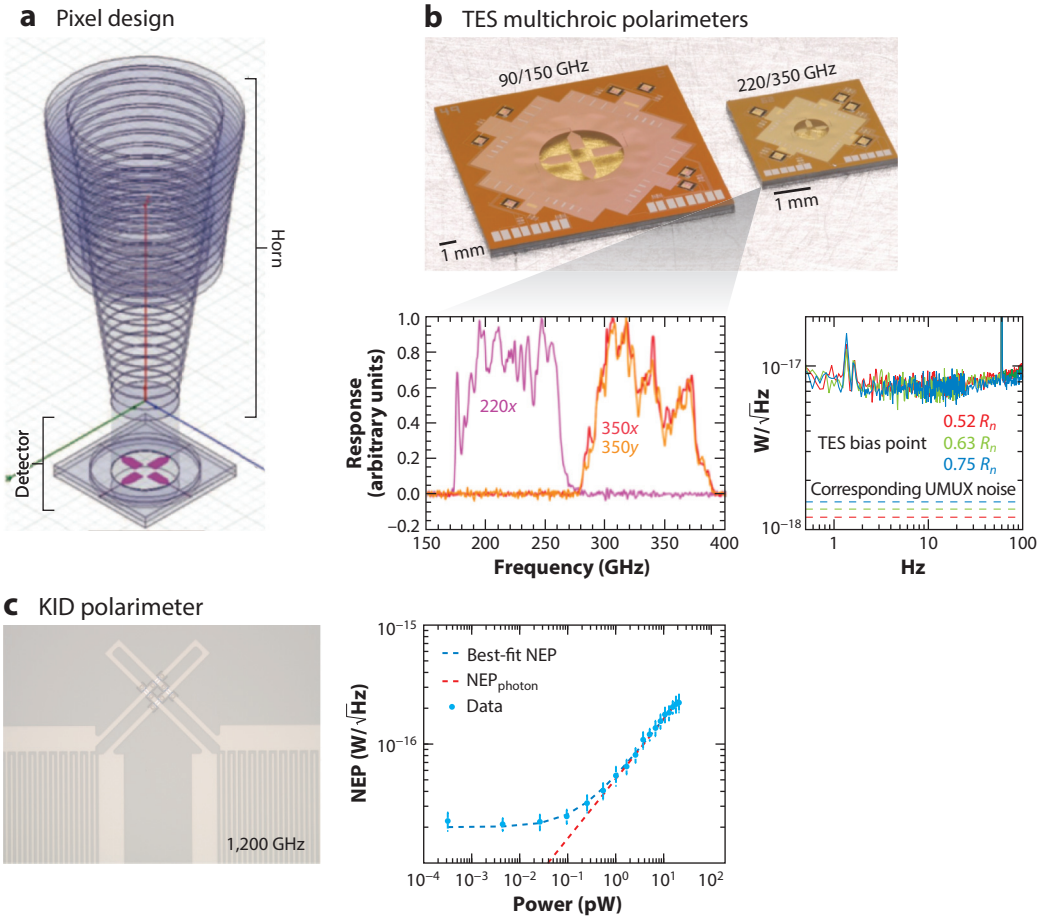

Figure 4

(*a*) Schematic of a single-mode horn coupled to a planar wave-guide probe orthomode transducer to separate the two incoming polarizations and couple them to planar microstrip lines (137). (*b*) (*Top*) Photographs of dual-polarization multichroic (dual-band) transition edge sensor (TES) detectors for cosmic microwave background measurements. (*Bottom left*) The measured frequency response of the different detectors from a single device. (*Bottom right*) The measured detector noise from a microwave multiplexed superconducting quantum interference device readout system coupled to a TES (138). (*c*) (*Left*) Photograph of a dual-polarization kinetic inductance detector (KID) prototype developed for measurements of submillimeter-wavelength polarized dust emission with the BLAST experiment (142). (*Right*) The measured noise as a function of absorbed optical power compared with the expected level of photon noise (145). Abbreviations: NEP, noise-equivalent power; UMUX, ultrahigh-frequency multiplexer.

systems. In TDM systems, the signal from each detector is read out sequentially with other detectors in a column. Detectors in each column are selected by sending address signals in sequence to each row of SQUID switches. In FDM systems, each detector has a cryogenic inductor-capacitor (LC) filter that defines a unique resonant frequency, f_0, and separates the signal from the other detectors in the frequency domain. For current FDM systems, the readout frequencies range from 0.1 to 10 MHz. The detectors are biased with a frequency comb corresponding to the set of filter

resonances, and the signals from all of the detectors are combined and read out continuously with a single SQUID amplifier.

A significant challenge for next-generation CMB experiments is scaling the readout electronics from current array sizes to one or two orders of magnitude more detectors. Currently, TES detectors are read out with multiplex factors (the number of detectors read out on a single line) of

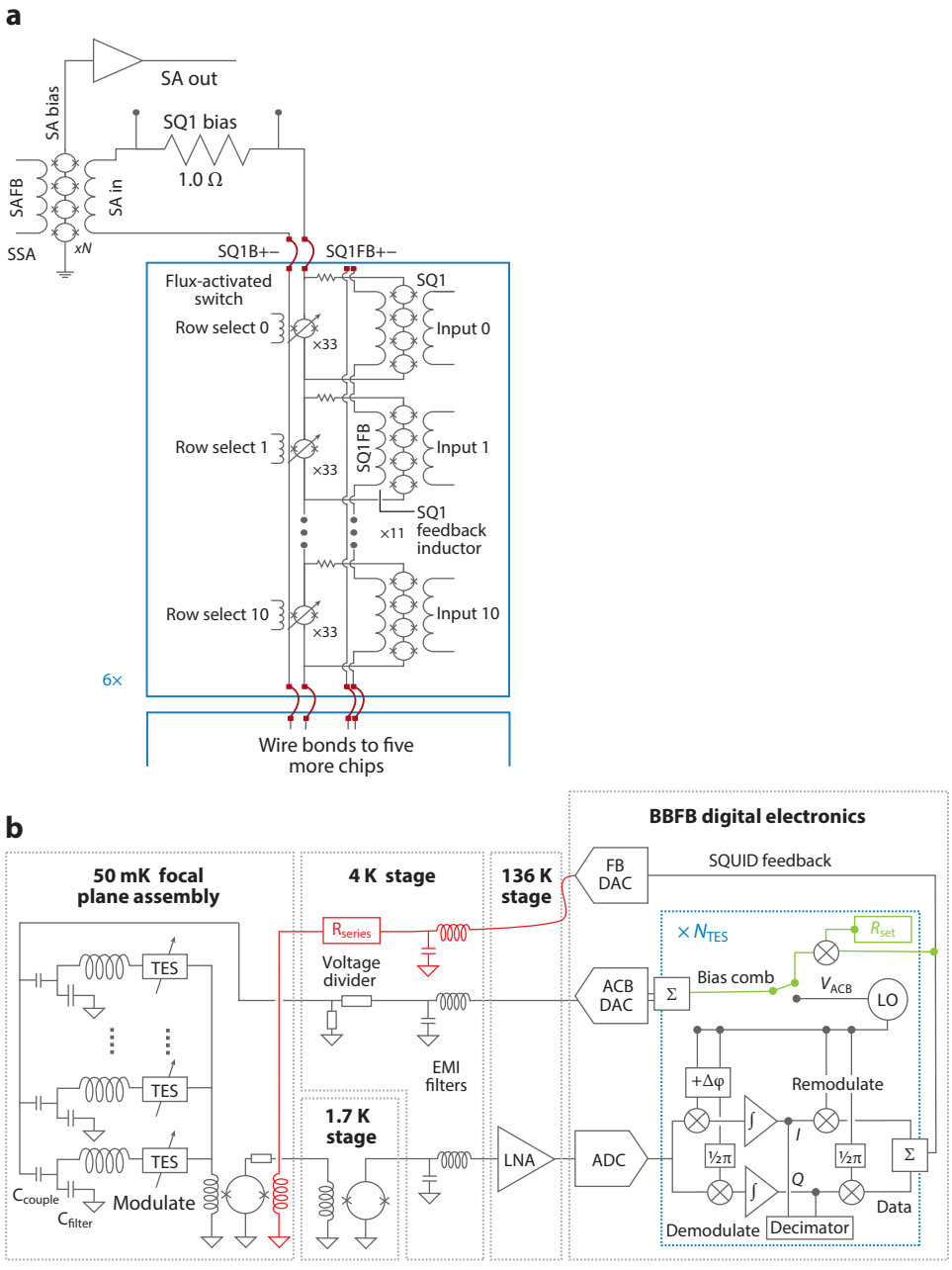

32–68 with both TDM (28, 129) and FDM (149, 150) systems. In order to keep the complexity and thermal input of the wiring comparable to those of existing systems, it is desirable to increase this multiplex factor significantly. Scaling up the existing TDM systems is challenging; for example, the TDM readout in the AdvancedACT-Pol experiments requires hundreds of multiplex chips and more than 20,000 wire bonds to read out 2,024 detectors (151). For this purpose, a relatively large area is required around the detector wafer, making tiling of focal planes into larger arrays difficult. The largest multiplexing factor demonstrated in the lab for FDM systems operating at megahertz frequencies is 176 (152). One promising way to increase the multiplex factor, called microwave multiplexing, involves scaling the FDM method by increasing the system bandwidth through the use of on-chip superconducting resonators coupled to SQUIDs that modulate their effective inductance in response to changes in current through the TESs (154). For resonant frequencies in the range of a few gigahertz, it is possible to multiplex on the order of 1,000 detectors on a single coaxial cable. This factor is similar to the multiplexing factors already achieved with KID arrays, and the associated electronics are also similar to those developed for KID readout.

5. FUTURE PROSPECTS

We anticipate that LTDs will provide compelling new results for DM and DBD searches within the next few years. The first 1-ton cryogenic DBD experiment is already taking data, demonstrating that masses as large as 1 ton can be easily operated at temperatures below 10 mK. DM LTDs show that the sub-keV energy threshold has now been reached, opening up new frontiers of sensitivity toward the $M_{\mathrm{wimp}} <$ few (GeV/c^2) parameter space. Research and development are ongoing, demonstrating the readiness of isotopically enriched DBD bolometers with heat–light readout for next-generation experiments and introducing new challenges in DM detector development in the energy threshold region below 100 eV.

The next generation of ground-based CMB experiments, including the recently established Simons Observatory and the planned CMB-S4 survey, aims to increase the CMB mapping speed by factors of 10–100 over that of current experiments. This increase will enable similar improvements in parameter space for the detection of primordial gravitational waves and constraints on inflation, measurements of the sum of neutrino masses, searches for light particle relics, and constraints on other fundamental physics parameters (155). Suborbital and space-based surveys will be needed to obtain complete spatial and electromagnetic frequency coverage of CMB anisotropies. Several

Figure 5

(*a*) Schematic for time-division multiplexing readout (151). Transition edge sensor (TES) detectors are coupled to a readout of superconducting quantum interference device (SQUID) series arrays along a column. All of the TES detectors are shunted by row-select SQUID switches, which are opened sequentially to send the signal from one TES detector at a time to the buffer amplifier and warm electronics. (*b*) Schematic for base-baseband feedback (BBFB) frequency-division multiplexing readout (150). Each TES detector is coupled to an inductor-capacitor resonant filter; they are biased in parallel with a frequency comb generated from a reference local oscillator (LO) that feeds the ac bias digital-to-analog converter (ACB DAC). The signals are read out with a cryogenic SQUID series array (SSA) amplifier that is kept at a fixed series array (SA) bias by use of a feedback (FB) flux signal from the FB DAC. The SQUID voltage is amplified by a second SQUID stage and a warm low-noise amplifier (LNA) and then digitized. The digital signals are downconverted to baseband, and the feedback signal is then computed inside the control electronics. Abbreviation: EMI, electromagnetic interference.

balloon-borne missions are ongoing or being proposed. In addition, several satellite missions are under study. For all of these experiments, careful control and characterization of experimental systematic effects, as well as removal of signal contamination from astrophysical foregrounds, will be needed. Fundamental to these efforts will be detailed optimization and characterization of LTD arrays.

DISCLOSURE STATEMENT

The authors are not aware of any affiliations, memberships, funding, or financial holdings that might be perceived as affecting the objectivity of this review.

LITERATURE CITED

1. Langley SP. *Proc. Am. Acad. Arts Sci.* 16:342–58 (1881)
2. White AD, Chanute O, Pickering EC. *Smithson. Misc. Coll.* 49:IV (1907)
3. Andrews DH, Fowler RD, Williams MC. *Phys. Rev.* 76:154 (1949)
4. Estermann I, Foner A. *Phys. Rev.* 79:365 (1950)
5. Low FJ. *J. Opt. Soc. Am.* 51:1300 (1961)
6. Klypin AA, Sazhin MV, Strukov IA, Skulachev DP. *Sov. Astron. Lett.* 13:104 (1987)
7. Schuster J, et al. *Astrophys. J. Lett.* 412:L47 (1993)
8. Hancock S, et al. *Nature* 367:333 (1994)
9. Smoot G, et al. *Astrophys. J.* 360:685 (1990)
10. Devlin MJ, et al. *Astrophys. J.* 509:L69 (1998)
11. Wollack EJ, et al. *Astrophys. J.* 476:440 (1997)
12. Scott PF, et al. *Astrophys. J.* 461:L1 (1996)
13. Miller A, et al. *Astrophys. J. Suppl.* 140:115 (2002)
14. Halverson N, et al. *Proc. SPIE* 3357:416 (1998)
15. Page LA, Cheng ES, Meyer SS. *Astrophys. J.* 355:L1 (1990)
16. Mather JC, Fixsen DJ, Shafer RA. *Proc. SPIE* 2019:168 (1993)
17. Fixsen DJ, et al. *Astrophys. J.* 470:63 (1996)
18. Devlin MJ, et al. *Astrophys. J. Lett.* 430:L1 (1994)
19. Crill BP, et al. *Astrophys. J. Suppl.* 148:527 (2003)
20. Rabii B, et al. *Rev. Sci. Instrum.* 77:071101 (2006)
21. Benoit A, et al. *Adv. Space Res.* 33:1790 (2004)
22. Mather JC, et al. *Astrophys. J.* 420:439 (1994)
23. Debernardis P, et al. *Nature* 404:955 (2000)
24. Hanany S, et al. *Astrophys. J. Lett.* 545:L5 (2000)
25. Ade PAR, et al. (Planck Collab.) *Astron. Astrophys.* 571:16 (2014)
26. Crites A, et al. *Astrophys. J.* 805:36 (2015)
27. Naess S, et al. *J. Cosmol. Astropart. Phys.* 10:007 (2014)
28. Ade PAR, et al. (BICEP2 Collab.) *Phys. Rev. Lett.* 112:241101(2014)
29. Ade PAR, et al. (POLARBEAR Collab.) *Astrophys. J.* 794:171 (2014)
30. Fiorini E, Niinikoski TO. *Nucl. Instrum. Methods A* 224:83 (1984)
31. Fukuda Y, et al. *Phys. Rev. Lett.* 81:1562 (1998)
32. Bernabei R, et al. *Phys. Lett. B* 424:195 (1998)
33. Klapdor-Kleingrothaus HV, et al. *Mod. Phys. Lett. A* 16:2409 (2001)
34. Agostini M, et al. *Phys. Rev. Lett.* 111:122503 (2013)
35. Twerenbold D. *Rep. Prog. Phys.* 59:349 (1996)
36. Booth NE, Cabrera B, Fiorini E. *Annu. Rev. Nucl. Part. Sci.* 46:471 (1996)
37. Quaglia R, et al. *IEEE Trans. Nucl. Sci.* 62:221 (2015)
38. Cardani L, et al. *J. Instrum.* 7:P01020 (2012)
39. Enns C, ed. *Cryogenic Particle Detection.* Berlin: Springer (2005)

40. Ullom JN, Bennet DA. *Supercond. Sci. Technol.* 28:084003 (2015)
41. de Marcillac P, et al. *Nature* 422:876 (2003)
42. Beeman JW, et al. *Phys. Rev. Lett.* 108:062501 (2012)
43. Casali N, et al. *J. Phys. G* 41:075101 (2014)
44. Raccanelli A, et al. *Cryogenics* 41:763 (2001)
45. Gorla P, Bucci C, Pirro S. *Nucl. Instrum. Methods A* 520:641 (2004)
46. Pirro S, et al. *Nucl. Instrum. Methods A* 444:331 (2000)
47. Mykkanen E, et al. *Rev. Sci. Instrum.* 87:105111 (2016)
48. Kalra R, et al. *Rev. Sci. Instrum.* 87:073905 (2016)
49. Wiener N. *Extrapolation, Interpolation, and Smoothing of Stationary Time Series with Engineering Applications*. Cambridge, MA: MIT Press (1964)
50. Gatti E, Manfredi PF. *Riv. Nuovo Cim.* 9:1 (1986)
51. Di Domizio S, Orio F, Vignati M. *J. Instrum.* 6:P02007 (2011)
52. Hehn L, et al. *Eur. Phys. J. C* 76:548 (2016)
53. Agnese R, et al. *Phys. Rev. Lett.* 16:071301 (2016)
54. Angloher G, et al. *Eur. Phys. J. C* 74:3184 (2014)
55. Caparelli S, et al. *Rev. Sci. Instrum.* 77:095102 (2006)
56. Riabzev SV, et al. *Cryogenics* 49:1 (2009)
57. Wang C, Hartnett JG. *Cryogenics* 50:336 (2010)
58. Pirro S. *Nucl. Instrum. Methods A* 559:672 (2006)
59. Schäffner K, et al. *Astropart. Phys.* 69:30 (2015)
60. Ligi C, et al. *J. Low Temp. Phys.* 184:590 (2016)
61. Alduino C, et al. *J. Instrum.* 11:P07009 (2016)
62. Barabash SA, et al. *Eur. Phys. J. C* 76:487 (2016)
63. Adam R, et al. (Planck Collab.) *Astron. Astrophys.* 594:A1 (2016)
64. Goodman MW, Witten E. *Phys. Rev. D* 31:3059 (1985)
65. Klasen M, Pohl M, Sigl G. *Prog. Part. Nucl. Phys.* 85:1 (2015)
66. Andi T, et al. (Panda-X Collab.) *Phys. Rev. Lett.* 117:121303 (2016)
67. Akerib DS, et al. (Lux Collab.) *Phys. Rev. Lett.* 118:021303 (2017)
68. Aprile E, et al. (Xenon Collab.) *Phys. Rev. D* 94:122001 (2016)
69. Agnes P, et al. (Dark-Side Collab.) *Phys. Lett. B* 743:456 (2015)
70. Aström J, et al. *Phys. Lett. A* 356:262 (2006)
71. Tantot A, et al. *Phys. Rev. Lett.* 111:154301 (2013)
72. Agostini M, et al. (GERDA Collab.) *Astropart. Phys.* 91:15 (2016)
73. Neganov BS, Trofimov NV. *Otkryt. Izobr.* 146:215 (1985)
74. Luke PN. *J. Appl. Phys.* 64:6858 (1988)
75. Armengaud E, et al. (Edelweiss Collab.) *J. Cosmol. Astropart. Phys*. 05:019 (2016)
76. Agnese R, et al. (SuperCDMS Collab.) *Phys. Rev. Lett*. 112:241302 (2014)
77. Haller EE, Palaio NP, Hansen WL, Kreysa E. In *Neutron Transmutation Doping of Semiconductor Materials*, ed. RD Larabee, p. 21. Boston: Springer (1984)
78. Agnese R, et al. (SuperCDMS Collab.) *Appl. Phys. Lett.* 103:164105 (2013)
79. de la Broïse X, Bounab A. *Nucl. Instrum. Methods A* 787:51 (2015)
80. Agnese R, et al. (SuperCDMS Collab.) *Phys. Rev. D* 95:082002 (2017)
81. Phipps A, et al. arXiv:1611.09712 [physics.ins-det] (2016)
82. Strauss R, et al. *Eur. Phys. J. C* 74:2957 (2014)
83. Angloher G, et al. *Eur. Phys. J. C* 76:25 (2016)
83a. Petricca F. *Direct dark matter search with the CRESST-III experiment*. Presented at Top. Astropart. Undergr. Phys. (TAUP), Sudbury, Can., July 24–28 (2017)
84. Strauss R, et al. *Nucl. Instrum. Methods A* 845:414 (2017)
85. Angloher G, et al. *Eur. Phys. J. C* 76:441 (2016)
86. Bernabei R, et al. *Eur. Phys. J. C* 73:2648 (2013)
87. Schäffner K, et al. *Astropart. Phys.* 84:70 (2016)
88. Avignone FT, Elliott SR, Engel J. *Rev. Mod. Phys.* 80:481 (2008)

89. Cremonesi O, Pavan M. *Adv. High Energy Phys.* 2014:951432 (2014)
90. Andreotti E, et al. *Astropart. Phys.* 34:822 (2011)
91. Alfonso K, et al. *Phys. Rev. Lett.* 115:102502 (2015)
91a. Cremonisi O. *First CUORE results.* Presented at Top. Astropart. Undergr. Phys. (TAUP), Sudbury, Can., July 24–28 (2017)
92. Bucci C, et al. *Eur. Phys. J. A* 41:155 (2009)
93. Pirro S, et al. *Phys. At. Nucl.* 69:2109 (2006)
94. Arnaboldi C, et al. *Astropart. Phys.* 34:143 (2010)
95. Gironi L, et al. *J. Instrum.* 5:P11007 (2010)
96. Arnaboldi C, et al. *Astropart. Phys.* 34:334 (2011)
97. Gironi L. *J. Low Temp. Phys.* 167:504 (2012)
98. Mikhailik VB, Kraus H. *Phys. Status Solidi B* 247:1583 (2010)
99. Arnaboldi C, et al. *Astropart. Phys.* 34:797 (2011)
100. Artusa DR, et al. *Eur. Phys. J. C* 76:364 (2016)
101. Beeman JW, et al. *Adv. High Energy Phys.* 2013:237973 (2013)
102. Kim GB, et al. *Adv. High Energy Phys.* 2015:817530 (2015)
103. Armengaud E, et al. *J. Phys. Conf. Ser.* 718:062008 (2016)
104. Broniatowski A, et al. *J. Low Temp. Phys.* 184:330 (2016)
105. Stark M, et al. *Nucl. Instrum. Methods A* 545:738 (2005)
106. Isaila C, et al. *Phys. Lett. B* 716:160 (2012)
107. Tabarelli de Fatis T. *Eur. Phys. J. C* 65:359 (2010)
108. Beeman JW, et al. *Astropart. Phys.* 35:558 (2012)
109. Willers M, et al. *J. Instrum.* 10:P03003 (2015)
110. Pattavina L, et al. *J. Low Temp. Phys.* 184:286 (2016)
111. Gironi L, et al. *Phys. Rev. C* 94:054608 (2016)
112. Artusa DR, et al. *Eur. Phys. J. C* 74:3096 (2014)
113. Artusa DR, et al. *Phys. Lett. B* 767:321 (2017)
114. Nucciotti A. *Adv. High Energy Phys.* 2016:9153024 (2016)
115. Drexlin G, et al. *Adv. High Energy Phys.* 2013:293986 (2013)
116. Alpert B, et al. *Eur. Phys. J. C* 75:112 (2015)
117. Giachero A, et al. *J. Instrum.* 12:C02046 (2017)
118. Hassel C, et al. *J. Low Temp. Phys.* 184:910 (2016)
119. Kempf S, et al. *AIP Adv.* 7:015007 (2017)
120. Ade PAR, et al. (Planck Collab.) *Astron. Astrophys.* 594:A13 (2016)
121. Ade PAR, et al. *Astrophys. J.* 806:206 (2015)
122. Austermann J, et al. *Proc. SPIE* 8452:84521E (2012)
123. Inoue Y, et al. *Proc. SPIE* 9914:99141I (2016)
124. Essinger-Heileman T, et al. *Proc. SPIE* 9153:91531I (2014)
125. Runyan MC, et al. *Proc. SPIE* 7741:77411O (2010)
126. Reichborn-Kjennerud B, et al. *Proc. SPIE* 7741:77411C (2010)
127. Lazear J, et al. *Proc. SPIE* 9153:91531L (2014)
128. Niemack MC, et al. *Proc. SPIE* 7741:77411S (2010)
129. Thornton RJ, et al. *Astrophys. J. Suppl.* 227:21T (2016)
130. Appel JW, et al. *Proc. SPIE* 9153:91531J (2014)
131. Swetz DS, et al. *Astrophys. J. Suppl.* 194:41 (2011)
132. Ade PAR, et al. (BICEP2 Collab.) *Astrophys. J.* 792:62 (2014)
133. Grace E, et al. *Proc. SPIE* 9153:915310 (2014)
134. Kermish ZD, et al. *Proc. SPIE* 8452:84521C (2012)
135. Shirokoff E, et al. *IEEE Trans. Appl. Supercond.* 19:517 (2009)
136. George EM, et al. *Proc. SPIE* 8452:84521F (2012)
137. Datta R, et al. *J. Low Temp. Phys.* 176:670 (2014)
138. Niemack M, et al. *J. Low Temp. Phys.* 184:746 (2016)
139. Monfardini A, et al. *Astron. Astrophys.* 521:A29 (2010)

140. Golwala S, et al. *Proc. SPIE* 8452:845205 (2012)
141. Swenson LJ, et al. *Proc. SPIE* 8452:84520P (2012)
142. Galitzky N, et al. *J. Astron. Instrum.* 3:1440001 (2014)
143. Barlis A, Aguirre J, Stevenson T. *Proc. SPIE* 9914:99142F (2016)
144. Flanigan D, et al. *Appl. Phys. Lett.* 108:083504 (2016)
145. Hubmayr J, et al. *Appl. Phys. Lett.* 106:073505 (2015)
146. de Korte PAJ, et al. *Rev. Sci. Instrum.* 74:3807 (2003)
147. Irwin KD, et al. *AIP Conf. Proc.* 605:301 (2002)
148. Dobbs MA, et al. *Rev. Sci. Instrum.* 83:073113 (2012)
149. Bender AN, et al. *Proc. SPIE* 9914:9914D1 (2016)
150. Rotermund K, et al. *J. Low Temp. Phys.* 184:486 (2016)
151. Henderson S, et al. *Proc. SPIE* 9914:9914G1 (2016)
152. Hijmering R, et al. *Proc. SPIE* 9914:99141C (2016)
153. Deleted in proof
154. Irwin KD, Lehnert KW. *Appl. Phys. Lett.* 85:2107 (2004)
155. Abazajian KN, et al. arXiv:1610.02743v1 [astro-ph] (2016)